

We are IntechOpen, the world's leading publisher of Open Access books Built by scientists, for scientists

6,900

Open access books available

185,000

International authors and editors

200M

Downloads

Our authors are among the

154

Countries delivered to

TOP 1%

most cited scientists

12.2%

Contributors from top 500 universities



WEB OF SCIENCE™

Selection of our books indexed in the Book Citation Index
in Web of Science™ Core Collection (BKCI)

Interested in publishing with us?
Contact book.department@intechopen.com

Numbers displayed above are based on latest data collected.
For more information visit www.intechopen.com



Mechanism and Prevention of Agglomeration/ Defluidization during Fluidized-Bed Reduction of Iron Ore

Yiwei Zhong, Jintao Gao, Zhancheng Guo and
Zhi Wang

Additional information is available at the end of the chapter

<http://dx.doi.org/10.5772/intechopen.68488>

Abstract

The mechanisms of agglomeration and defluidization and fluidization characteristic of iron oxide particles were investigated based on the theory of surface diffusion, interface reaction, surface nano/microeffect, and phase transformation. Moreover, a mathematical model was developed to predict the high-temperature defluidization behavior by the force-balance and plastic-viscous flow mechanism, and the fluidization phase diagram was obtained. On these bases, a control method of defluidization and its inhibition mechanism were proposed. As a result, the theoretical system of agglomeration/defluidization in the gas-solid fluidization was developed, and thus afforded theory support and technological bases for the solution of defluidization in industrial fluidized-bed reactors.

Keywords: fluidized-bed reduction, iron ore, agglomeration, defluidization, prevention, model

1. Introduction

Fluidized-bed reactors can improve the reaction kinetics and realize better utilization of resource/energy and lower pollutant emissions [1]. Therefore, as a trend in the industrial application, fluidized beds are ideally suited to the processing of these finely sized raw materials and have great competitiveness. However, fluidized beds were tested but failed because of the serious problem of particles agglomeration and subsequent defluidization [2]. The continuous operation and high productivity was often limited by partial or complete defluidization. It is, therefore, a critical problem to solve defluidization and particle agglomeration at high temperatures for the application of fluidized beds.

Particle agglomeration in fluidized-bed systems has received considerable attention due to its close association with industrial processes. Gluckman [3] indicated that the generation of agglomerations depended on the cohesiveness of particles collisions. Seville and coworkers [4, 5] pointed that the defluidization phenomenon was attributed to an increased rate of sintering at elevated temperatures, and the tendency of particle to agglomerate depended strongly on their physical and chemical characteristics at high temperature. Two types of adhesion are considered [4–7]: (1) Visco materials cause sintering on glassy materials. Increasing the operating temperature can reduce the viscosity of the materials and cause a larger adhesive force. (2) Melting and chemical reaction produces liquid-phase materials. These liquid-phase materials can form a bridge between two particles and cause agglomeration and defluidization.

In the case of fluidized-bed reduction of iron ore, earlier works [8–10] indicated that sticking occurred mostly during metallization of ore. The defluidization tended to be preferred at a high fractional reduction and metallization degree. Some ore particles were precipitated by the metal iron with the fibrous shape on the particle surface. The sticking was initiated by the contact of the needles that hooked mechanically the particles together. Moreover, the work of Gransden et al. [9, 10] showed that the sticking was associated with the iron-iron contact regardless of formation of iron whiskers or not. They believed that the fresh precipitated iron had a high activity or surface energy, and thus appeared high adhesion energy to agglomeration. Zhong et al. [11] also reported agglomerates formed due to sintering of reduced iron, and nano/microstructure on the particle surface had a promotive effect on particle agglomeration. Therefore, the sticking tendency depended strongly on iron precipitation of particles. With respect to adhesion of metallic iron, a sintering mechanism of iron particles has been reported involving the relationship between the bed temperature and the minimum gas fluidizing velocity required to prevent defluidization [12, 13]. However, most research studies focused on the metallic iron content and morphologies at the defluidization point [2, 8–11] and thus did not involve the evolution of particle properties during metallization. In the gas-solid reaction, new components were produced and thus caused the changes in surface structure and the particle properties. Therefore, the new phase formation can significantly affect the particle cohesiveness.

2. Mechanism of agglomeration and defluidization of iron/iron oxide particles

2.1. Effect of metallization degree on agglomeration tendency

The fluidized-bed apparatus is shown in **Figure 1**, which is a bubbling fluidized bed consisting of a transparent silica tube with an inner diameter of 2.5 cm. The reactor is heated by a transparent electric resistance, and the fluidization state in the reactor can be observed at high temperature. Bed temperature is measured and controlled by a PID controller connected with a K-typed thermocouple. The gas flow rate and pressure drop across the bed is measured by a digital mass flow meter and a pressure transmitter, respectively. The pressure sensor is located at 1 cm below the gas distributor.

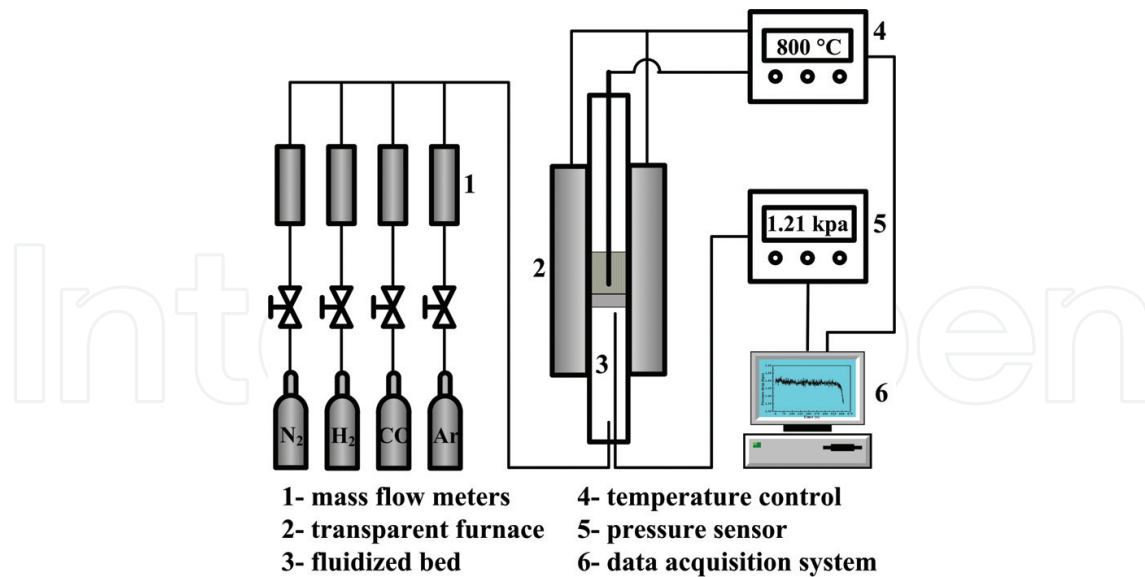


Figure 1. Schematic diagram of fluidized-bed apparatus.

To determine the evolution of the real-time bed agglomeration tendencies and agglomeration potential, the controlled bed defluidization tests (CBD) were carried out, which were adapted from Öhman [14, 15]. Each experiment with a 5 g of iron oxide was started by a normal fluidized-bed reduction by CO at 700°C (1.0 NL/min, about 12.2 cm/s) to obtain a series of reduced samples with different metallization degrees (M_{Fe}). Preliminary reduction experiments indicated that when M_{Fe} was higher than 25%, the bed agglomeration would appear. Thus, M_{Fe} of all the reduced samples was controlled below 25%. And then at a point where a designated metallization degree was achieved by controlling the reducing time, the reduction was stopped and the fluidizing gas was switched to N₂ atmosphere (1.0 NL/min, about 12.2 cm/s). Then, the bed was heated up at a rate of 3°C/min until a bed agglomeration was achieved. The bed defluidization temperature, T_{def} was determined by online analysis of the variations in the measured bed temperatures and differential pressures and was used to characterize bed agglomeration tendency at various metallization degrees. Defluidization is defined as any condition where a well-fluidized bed loses fluidization, whether partial or total [16]. A typical illustration of fluctuations in temperatures and differential bed pressures versus time in a controlled bed defluidization test is shown in Figure 2. Meanwhile, the controlled bed defluidization tests can also be carried out as a series of interrupted experiments to investigate the evolution of particles in the course of metallization.

The real-time agglomeration tendency of the reduced samples represented by the defluidization temperature T_{def} was obtained by the controlled bed defluidization tests. As shown in Figure 3, the defluidization temperature decreases with the increase of the metallization degree, indicating an increase of agglomeration tendency. The analysis of XRD (X-ray diffraction) shows that all the reduced samples in the controlled defluidization tests only contain metallic iron and FeO (Figure 4). The diffraction peaks of metallic iron obviously strengthened with increasing reduction time, indicating the content of precipitated iron increased. Therefore, the agglomeration tendency depended strongly on the metallic iron content. At the metallization degree

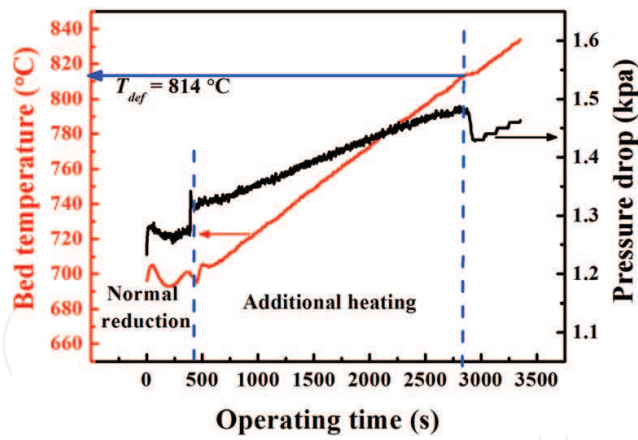


Figure 2. Illustration of a typical controlled defluidization test for Fe₂O₃ reduction.

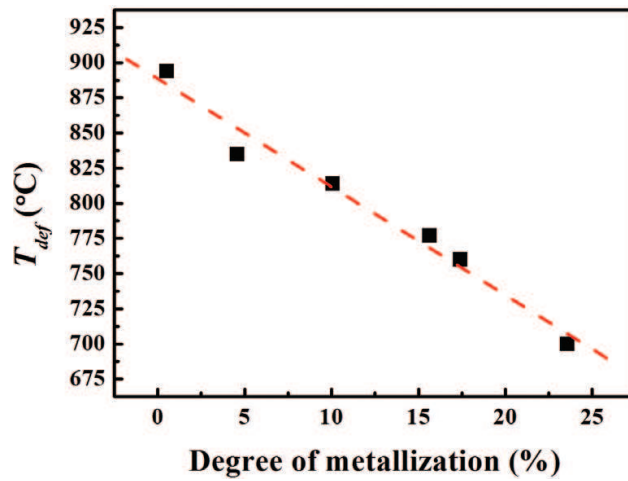


Figure 3. Influence of metallization degree on the defluidization temperature in the controlled defluidization tests.

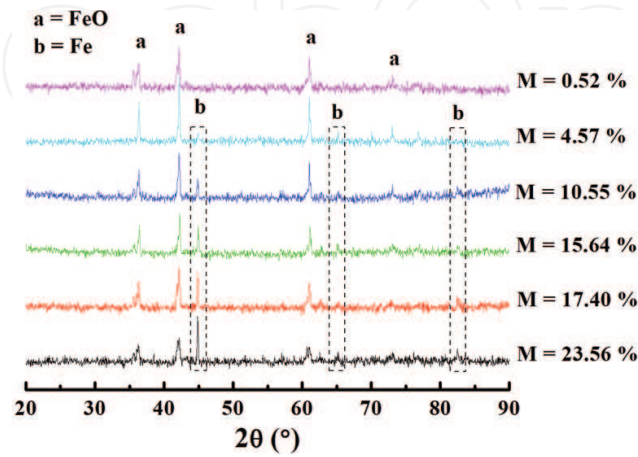


Figure 4. X-ray patterns of each sample from the controlled bed defluidization tests.

below 0.52%, no indication of defluidization is observed. This was because that the particle with lower amount of precipitated iron did not have enough adhesion force to form agglomerates and thus maintained a good quality of fluidization. When the metallization degree reached to 23.56%, the defluidization approached, indicating the defluidization was accompanied with the accumulation of precipitated iron. This result suggested that large quantities of metallic iron can increase the stickiness of particles by providing enough contact area of iron. This conclusion was in accord with that found by Gransden et al. [9, 10], who indicated that the agglomeration was caused by the iron-iron contact. Therefore, the reduced Fe_2O_3 particle with a higher metallization degree had a larger agglomeration tendency.

Typical morphologies of reduced samples at various metallization degrees are shown in **Figure 5**. At lower metallization degree (i.e., <4.57%), numerous pits are formed on the oxide surface prior to iron nucleation, and the morphology presents smooth. But at higher metallization degree (i.e., >15.64%), the iron nuclei tend to appear (about 0.1–0.15 μm in a diameter), forming microconvexities on the surface. These iron nuclei with nano/microsize were prone to soften and sinter together due to a higher surface energy [11]. Thus, the reduced particles with a higher metallization degree had a stronger adhesive force for agglomeration. On the other hand, the particle surface becomes rough due to the formation of iron nuclei. Such rough surface caused the enhancement of friction force among bed particles to result in a poor fluidization quality.

2.2. Effect of iron precipitation on particle cohesiveness

To investigate the evaluation of particle cohesiveness responsible for agglomeration, the thermomechanical analysis (TMA) was carried out by a dilatometer (NETZSCH-DIL402C,

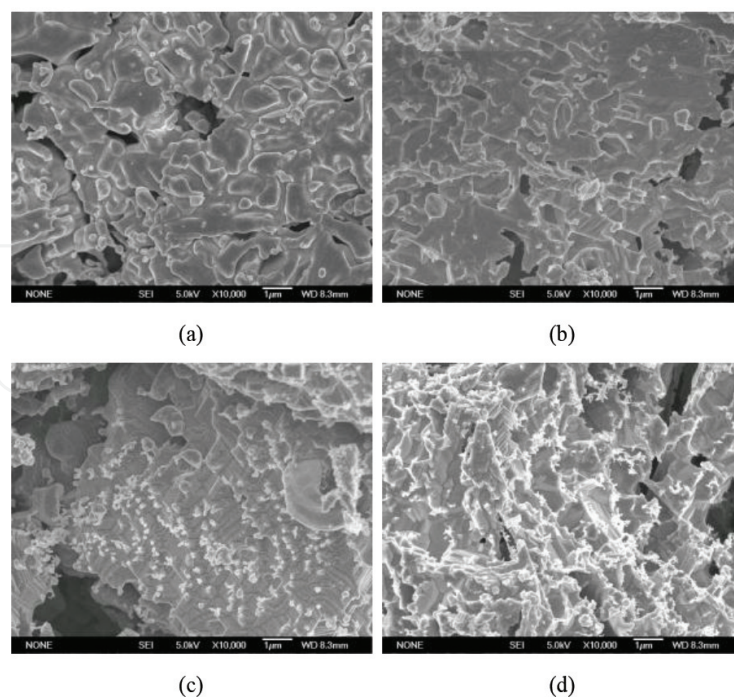


Figure 5. Evolution of surface morphology of Fe_2O_3 particles in the controlled defluidization tests: (a) $M_{\text{Fe}} = 0.52\%$; (b) $M_{\text{Fe}} = 4.57\%$; (c) $M_{\text{Fe}} = 15.64\%$; and (d) $M_{\text{Fe}} = 23.56\%$.

Germany). The thermal expansion or contraction was measured to obtain the temperature at which sintering and surface softening became significant. The sample was heated up to 800°C at a rate of 10°C/min. The sample was in a flow of 50 ml/min of pure Ar, and the load on it was 30 cN.

The samples from the controlled bed defluidization tests were examined. The greatest change in $\Delta L/\Delta L_0$ gradient for each curve is a measure of the minimum sintering temperature (T_s) [4, 5]. As shown in **Figure 6(a)**, the sample with a higher metallization degree has a lower value of T_s . This result showed that iron precipitation reduced significantly the minimum sintering temperature of the whole particle and thus enhanced the sintering activity of the reduced particle. The sintering rate depended on the diffusion coefficient (D_s) of materials. The value of D_s for α -iron self-diffusion was calculated to be approximately 10 times larger than that for the diffusion of Fe in FeO at 800°C according to the empirical correlations [17, 18]. This indicated that metallic iron had a higher sintering activity than FeO. Therefore, the tendency of the reduced particles to sinter together was intensified due to iron precipitation.

Many investigations showed the importance of the initial sintering temperature in fluidization quality [4, 5], because it is an indicator of the onset of agglomeration and is a softening point where the rate of sintering dramatically accelerated. Previous research studies [4, 5] have confirmed that the cohesiveness and sintering of the fluidized particles can lead to the uncontrolled particle agglomeration and subsequent defluidization at temperatures at or above the sintering point. A special class of agglomeration was due to the formation of new species on the surface of the solid particle during a chemical reaction. At temperatures well below the softening (sintering) points of both the reactants and the products, particle agglomeration can occur during the process of product formation [19]. Accordingly, in the case of reduction Fe_2O_3 to Fe, when metallic iron formed above sintering temperature, the adhesive force due to sintering was increased. Therefore, the sintering of metallic iron on the surface provided favorable conditions for agglomeration.

At the minimum sintering temperature (T_s), the surface of material began to soften and deform, and the surface stickiness began to appear [20, 21]. And the agglomeration and defluidization occurred as a result of having “sticky” bed materials. In this study, the surface viscosities of the reduced samples in the controlled bed defluidization tests at various metallization degrees were

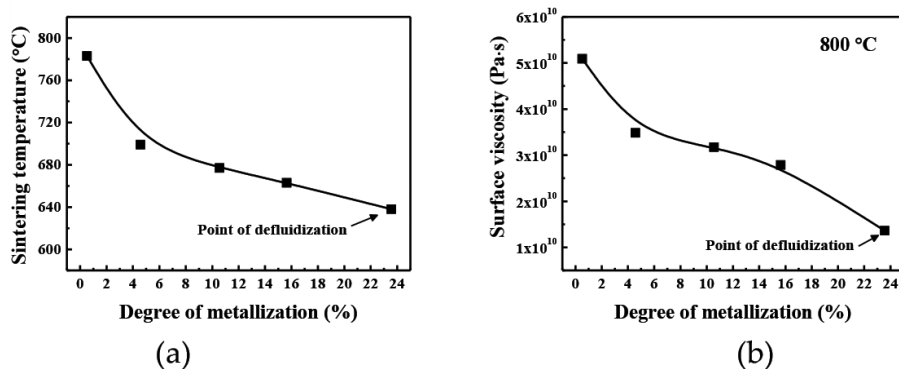


Figure 6. Influence of iron precipitation on particle cohesiveness of reduced Fe_2O_3 particles: (a) the minimum sintering temperature; (b) the surface viscosity of Fe_2O_3 particles at 800 °C).

measured at 800°C using the thermomechanical analysis as reported by Tardos [20]. **Figure 5(b)** shows that the surface viscosities gradually decreased as the metallization degree increased. When the metallization degree approaches to 23.56% (point of defluidization), the viscosity drops significantly, indicating a strong surface softening and stickiness of particles. This result suggested that the particle adhesion of iron oxide was enhanced with the increase of the amount of metallic iron on the surface.

For crystalline materials, the Huttig temperature is defined as the temperature where the lattices and surface atoms become appreciably mobile. For pure metals, this temperature was approximately $0.3T_m$ (about 330°C for iron) [22]. It was inferred that the Fe_2O_3 particle surface preformed viscosity because of the iron precipitation when the temperature was higher than 330°C. This fresh precipitated iron had high particle cohesiveness due to the higher activity and surface energy [8–11]. In the course of Fe_2O_3 reduction, numerous Fe vacancies were formed, and iron atoms were released from the oxide lattice due to oxygen removal. Consequently, the migration of iron atoms to the reducing front through Fe vacancies was accelerated due to the chemical potential gradient of O/Fe [23]. Therefore, the particle surface softened as metallic iron precipitating, resulting in a decrease of apparent surface viscosity.

Some of the agglomerates, sampled from controlled bed defluidization tests, were examined by SEM/EDS analysis. As seen in **Figure 7**, sintered necks instead of iron whiskers were observed between particles. The reduced particles are stucked together by the sintered neck, the diameter of which was roughly 0.8 μm . The EDS analysis showed that Fe was the dominant species (97 wt.%) in the connect position. Thus, the reduced particle was connected by a connective bridge composed of metallic iron. These results proved that the presence of iron, rather than iron oxide (FeO , Fe_3O_4), caused the formation of the sticky particle surfaces readily for agglomeration. In addition, it was noted that the agglomerates contained particles only several microns in diameter between coarse particles. These fine particles played a role of “bridge” in the formation of agglomerates.

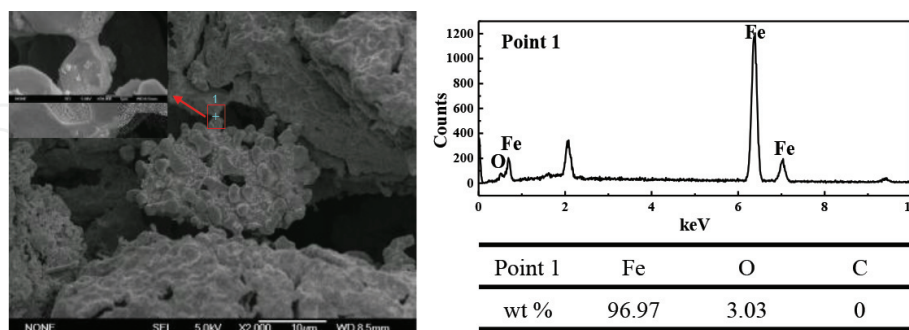


Figure 7. SEM image and EDS analysis of agglomerate sample at metallization degree of 15.64%.

3. Model to predict agglomeration and defluidization

The aim of this work is modeling the high-temperature defluidization behavior of iron powders involving the effects of gas velocity and gas properties. The calculation is focused on the

evolution of forces acting on particles with temperature based on the surface viscosity and bubble motion. By analyzing the experimental data with a statistical regression, a force balance model is developed to describe the defluidization processes in a fluidized bed, by which the temperature dependence of the defluidization behavior is predicted.

3.1. Modeling defluidization phenomena

3.1.1. Assumptions

The fluidization behavior of bed particles depended on the forces acting on them. Therefore, this model employed the balance of cohesive and segregate forces to simulate agglomeration/defluidization and predict the defluidization temperature. Taking account of particle moving, colliding, coalescing, and breaking in a fluidized-bed system, the following assumptions are made to describe the main characteristics of the defluidization phenomena based on the previously described experimental results:

1. Bed material particles are spherical and in uniform size.
2. The fluidizing gases do not react with the bed particles, and no coating layer form on the surface.
3. The adhesive force between two particles arises from surface viscosity and is determined by the plastic-viscous flow mechanism.
4. The force against agglomeration is the drag force acted on particles due to bubble motion.
5. If the adhesive force equals or exceeds the segregation force, the bed defluidization appears.

3.1.2. Model formulation

As the temperature increases, the effect of adhesion force becomes dominant due to surface softening, resulting in a quick defluidization. The adhesive force associated with the plastic-viscous flow mechanism can be described by:

$$F_{\text{ad}} = \pi b^2 \sigma \quad (1)$$

where σ represents the tensile stress of the agglomerate and b is the radius of the connection between the particles.

According to Benson et al. [24], the tensile stress of the agglomerate is

$$\sigma = \frac{At}{\mu_s d_p} \quad (2)$$

where A is a constant; t represents the connect time of two particles; d_p is the mean size of the particle; and μ_s is the surface viscosity of the particle materials.

In a fluidized bed where particles are intermittently mixed, the contact time of particles is dependent on the bubbles motion. The residence time is required to be sufficiently long for particle connection to form agglomerates. Therefore, in this study, the connect time of two

particles was considered as the characteristic residence time for which particles within a fluidized bed remain in contact with each other as reported by Seville et al. [13, 25]:

$$t = \frac{\beta}{(U_g - U_{mf})} \quad (3)$$

where β is a proportional coefficient; U_g is the operating gas velocity; and U_{mf} is the minimum fluidization velocity.

The surface viscosity of solid is a function of temperature and is assumed be estimated by the Arrhenius' expression [25]:

$$\mu_s = \mu_{s0} \exp\left(\frac{E_s}{RT}\right) \quad (4)$$

where E_s is the activation energy for the surface viscosity and T the absolute temperature.

To accurately predict the segregate force, this model employs the drag force acting on particles to represent the force against agglomeration, which is related to the effect of the particle size, gas velocity, and gas properties. The expression is [26]:

$$F_d = \alpha C_d \frac{\pi}{8} d_p^2 \rho_g U_g^2 \quad (5)$$

$$C_d = \frac{24}{Re} (1 + 0.173 Re^{0.657}) + \frac{0.413}{1 + 16300 Re^{-1.09}} \quad (6)$$

$$Re = \frac{d_p \rho_g U_g}{\mu_g} \quad (7)$$

where α is a proportional coefficient, representing the unknown errors in this equation. C_d is the drag coefficient; Re is Reynolds number; ρ_g and μ_g are the gas density and viscosity, respectively.

If the adhesive force equals the drag force, the bed is defluidized:

$$\frac{\pi A \beta b^2}{\mu_s d_p (U_g - U_{mf})} = \alpha C_d \frac{\pi}{8} d_p^2 \rho_g U_g^2 \quad (8)$$

In this work, we defined two number groups, N_a and N_d , representing the adhesion force and the drag force, respectively:

$$N_a = \frac{\pi}{\mu_s d_p (U_g - U_{mf})} \quad (9)$$

$$N_d = C_d \frac{\pi}{8} d_p^2 \rho_g U_g^2 \quad (10)$$

Therefore, the defluidization criterion (Eq. (8)) can be expressed as:

$$N_a = K \cdot N_d \tag{11}$$

$$K = \frac{\alpha}{Ab^2\beta} \tag{12}$$

where K is a regressive constant, representing the unknown errors in this equation. The variables in the model are as a function of temperature, and the correlations are nonlinear. Therefore, by combining Eqs. (9)–(12), the temperature to reach defluidization was obtained by a numerical method.

3.2. Modeling results and comparison with experimental data

3.2.1. Influence of gas velocity

Figure 8 presents the results obtained at different gas velocities. According to the definition of defluidization criterion, the temperature corresponding to the intersection of the curves of N_a and $K \cdot N_d$ is the defluidization temperature. As it can be seen, the temperature to reach defluidization increases with increasing the gas velocity for all the fluidizing gases. In previous studies [27–29], the generation of agglomeration and defluidization depended on the balance of the cohesive and breaking forces. And if the adhesive force between particles exceeded the breakage force, agglomeration and defluidization in the bed probably occur. As shown in

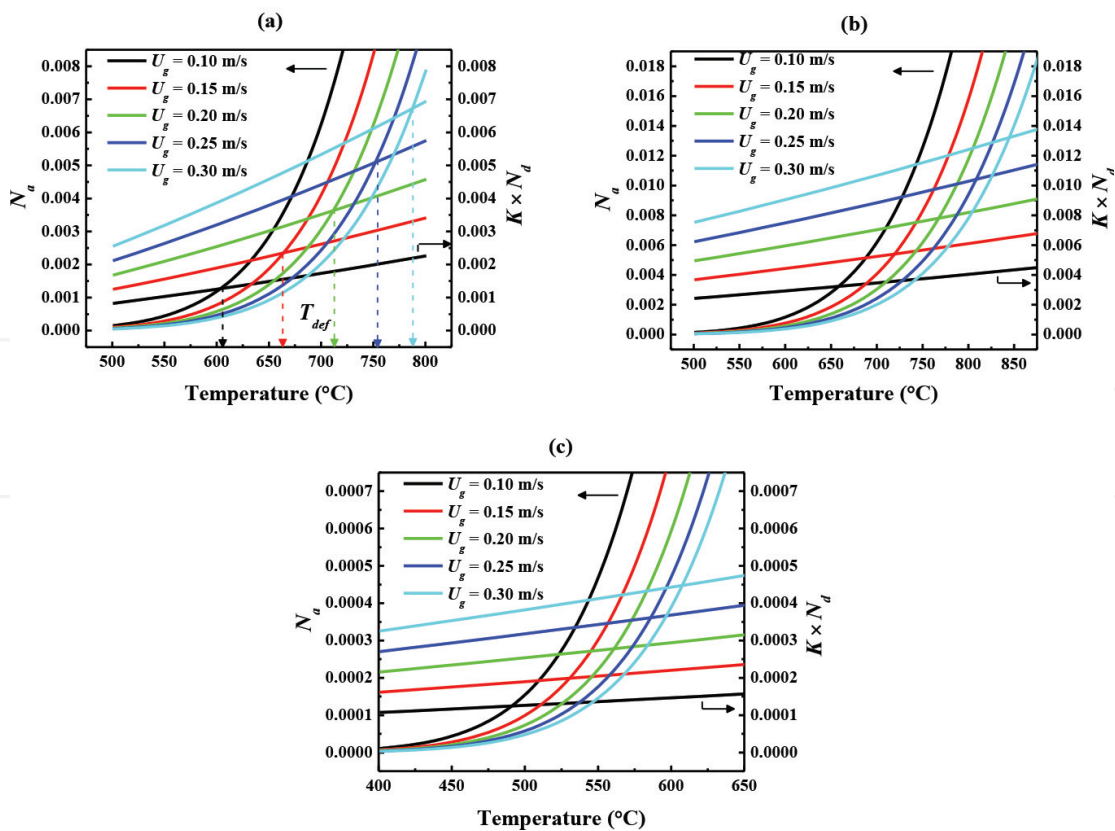


Figure 8. The variation of the calculated values of N_a and $K \cdot N_d$ with temperature: (a) N_2 ; (b) Ar; and (c) H_2 .

Figure 8, at a constant fluidizing velocity, both the adhesion force and the drag force increase with increasing temperature. However, the increase of adhesion force is much more rapid than that of drag force, especially at the temperatures above the initial sintering temperature. Therefore, at a given temperature, namely, the defluidization temperature, the adhesion force begins to be greater than the drag force, and thus the defluidization appears. This explained the temperature dependence of defluidization behavior. On the other hand, as the gas velocity increases, the drag force of the particles increases, whereas the adhesion force decreases at a constant temperature. As a result, the state of fluidized particles gets out of the defluidization region because the drag force is greater than the adhesion force. Therefore, the temperature to reach defluidization is delayed by increasing the gas velocity. Comparing the calculated defluidization temperature with the experimental data in **Figure 9(a)**, both the tendencies are in a good agreement, although the calculated values are to some extent lower than the experimental ones.

3.2.2. Influence of gas properties

Figure 9(b) presents the effect of gas type on defluidization temperature. According to the calculated results, the defluidization temperature decreases when using the gas with greater viscosity and density as a fluidizing agent. As seen in **Figure 9(b)**, at a constant gas velocity the adhesion force for different gases almost has no change, whereas the drag force is strongly dependent on the gas properties and increases with increasing the gas viscosity. Comparing the three fluidizing gases, the defluidization temperatures are in the following sequence: $H_2 < N_2 < Ar$. This was because the fluidizing gas with greater viscosity can produce a stronger drag force to resist agglomeration, which was in accord with the experimental results [21].

The calculated defluidization temperatures were in a good agreement with the experimental results in all experiment conditions, and thus confirmed the predicted modeling. The model successfully described the defluidization temperature as a function of gas velocity and gas property. According to the results above, the fluidizing phase diagram was obtained as shown in **Figure 10**, which was divided into the stable fluidization and the defluidization region. The fluidization state was maintained below the curve intersection of N_a and $K \cdot N_{dr}$, while the bed was defluidized above the intersection. This suggested that at a certain operating parameter,

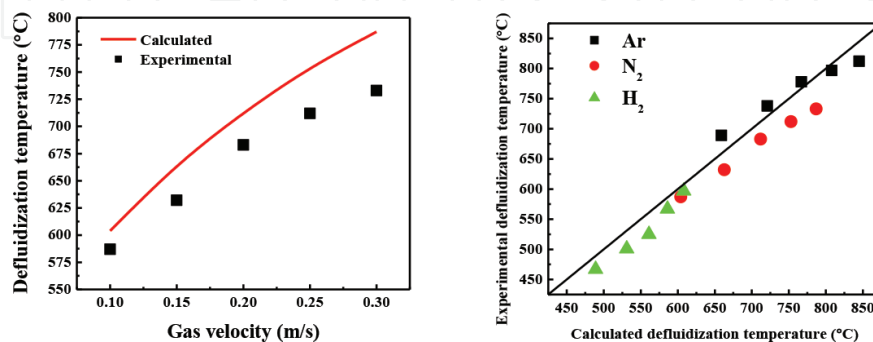


Figure 9. Comparison of calculated defluidization temperature with experimental data: (a) Influence of gas velocity; and (b) influence of gas properties.

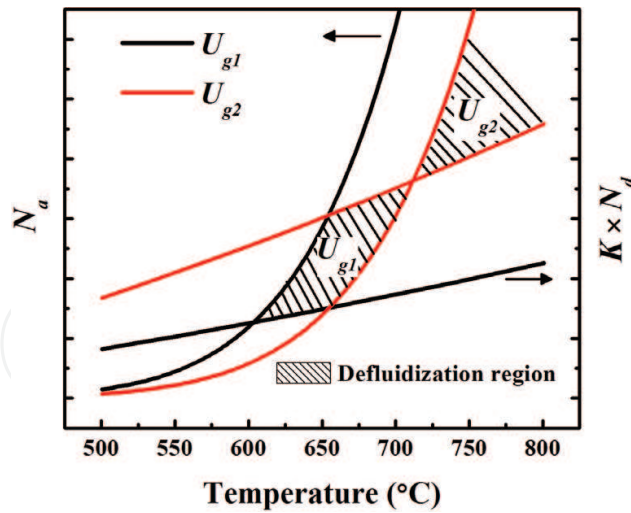


Figure 10. The fluidization phase diagram of iron powders at elevated temperatures.

there was a limiting operating temperature and gas velocity, above which the defluidization occurred. Therefore, the model can be considered as a theory reference to avoid defluidization in the actual fluidizing operations. However, the model cannot simulate the agglomeration involving chemical reaction and phase transformation. More work is needed for a comprehensive model of agglomeration in a fluidized-bed reactor.

4. Prevention of agglomeration by surface coating of Mg and Ca oxides

4.1. Effect of MgO and CaO addition on defluidization

Figure 11 shows the effects of the addition of MgO and CaO on the defluidization time of Fe₂O₃ particles at various operating temperatures. It was found that adding Mg and Ca had the similar effect on prolonging the defluidization time. As the addition content of MgO and CaO increased, the defluidization time was delayed. The defluidization time of adding MgO

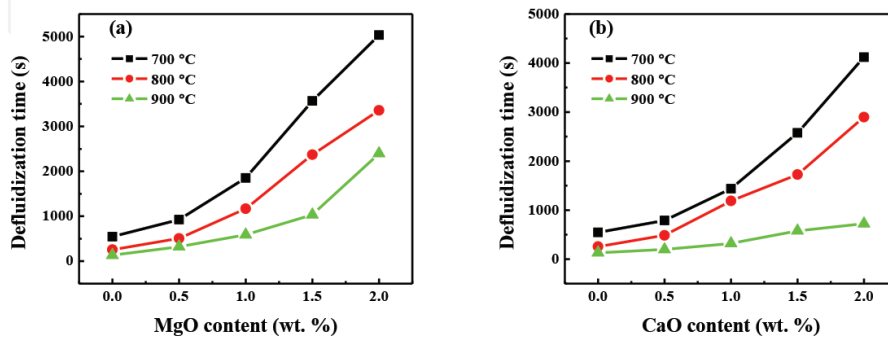


Figure 11. Influence of operating temperature on the defluidization time (50–74 μm, 36.5 cm/s): (a) adding MgO and (b) adding CaO.

are higher than that of adding CaO. It was indicated that MgO species had a better effect to reduce the bed agglomeration tendency and inhibit the defluidization.

However, previous research studies suggested that some compounds with low melting points or iron whiskers were formed by adding MgO and CaO. These compounds and iron whiskers provided a favorable condition to form agglomeration of the Fe_2O_3 particles during reduction [8, 30]. With inconsistent results as compared to those of the experiment, this work was focused on investigating the relationship between the new phase formation and particle adhesion during Fe_2O_3 reduction. It has been confirmed that agglomeration at high temperature was attributed to the activity of metallic iron [10, 21]. The surface energy of precipitated iron may be deactivated or reduced by Mg/Ca oxide, and thus the surface cohesiveness was eliminated. On the other hand, MgO and CaO may react with Fe_2O_3 to generate some eutectics with high melting points or some stable compounds hard to be reduced to metallic iron. In these conditions, the formation of liquid phase and the connection of metallic iron on the surface can be avoided at high temperature. Therefore, MgO and CaO inhibited the formation of agglomeration and delayed the defluidization time.

4.2. Behaviors of Mg and Ca species during reduction

In previous studies [31, 32], the formation of coating layer and connective bridge among the bed particles had been found based on the SEM (scanning electron microscopy)/EDS (energy dispersive spectrometry) analysis. However, in the case of no liquid phases, the physicochemical behavior of Mg/Ca species on the surface and their effects on the bed particles has not been determined yet. Therefore, the focus was the role of Mg and Ca species in the formation of the coating layer. The surfaces of bed particle samples were analyzed by SEM/EDS after the test at

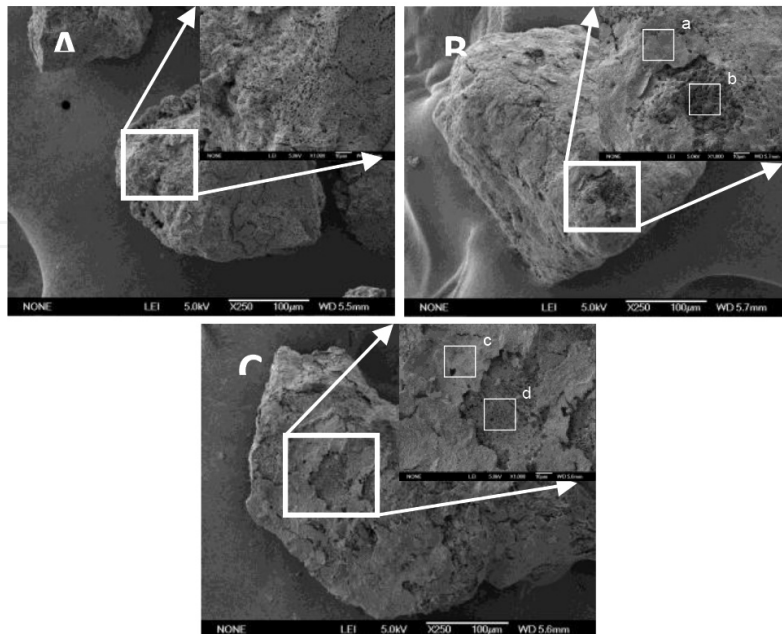


Figure 12. The SEM images of reduced particles (800°C , $74\text{--}149\ \mu\text{m}$, $24.3\ \text{cm/s}$): (a) no additive; (b) adding 2% MgO; and (c) adding 2% CaO.

the bed temperature of 800°C. As shown in **Figure 12(a)**, the morphology of sample was porous when no MgO or CaO was added, and many tiny iron grains appeared on the surface. But the bed particles were covered by the local coating layer when adding MgO and CaO (**Figure 12(b)** and **(c)**). And no obvious iron whiskers and substance in molten state were found on the surface, which was inconsistent with the results suggesting cation additions promoted fibrous iron [33, 34]. The reason was that the growth of iron whiskers was suppressed due to the formation of coating layer. The EDS spot analysis (**Figure 13(a)** and **(c)**) shows that the compositions of this coating layer were not only Mg and Ca but also large amount of Fe. It was inferred that this layer consisted of some complex compounds where Fe_2O_3 were not reduced completely. However, unlike the coating layer, the uncoated surface appears the porous morphology. The EDS analysis (**Figure 13(b)** and **(d)**) show that the compositions of the uncoated surface were element Fe, suggesting that metallic iron was precipitated under the coating layer. This was because that the coating layer was porous and cracked, and thus the external/internal diffusion for Fe oxides was easy. The metallization in bulk was slightly affected by surface coating. Therefore, it was inferred that the coating layer behaved like shell structure and inhibited the precipitated iron to expose on the surface of bed particle. The coating layer formed by adding MgO and CaO had a suppressive effect on defluidization and agglomeration.

To further identify the formation of new phase of Mg or Ca compounds during the reduction, the dominant species in the agglomerates was analyzed by XRD. **Figure 14** shows the phase composition with adding MgO and CaO before and after reduction. Before reduction the bed particles contained mainly Fe_2O_3 and a little $\text{MgO}\cdot\text{Fe}_2\text{O}_3$. However, after reduction a great number of metallic irons were observed, and the Mg and Ca species were in the formation of $\text{MgO}\cdot\text{FeO}$ and $\text{CaO}\cdot\text{FeO}$. Mg and Ca species can react with Fe_2O_3 to generate magnesium ferrite and calcium ferrite after pretreatment at 400–700°C [35], and these Fe compounds can

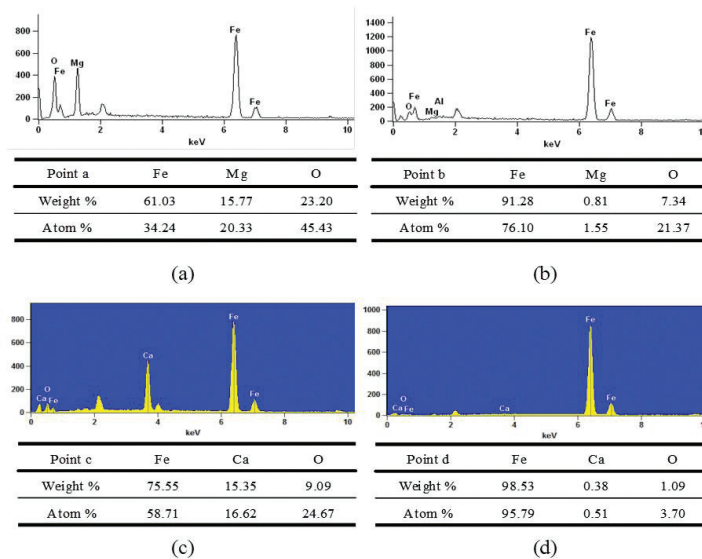


Figure 13. The EDS spot analysis of reduced particles (800°C, 74–149 μm , 24.3 cm/s): (a) Point a; (b) Point b; (c) Point c; and (d) Point d.

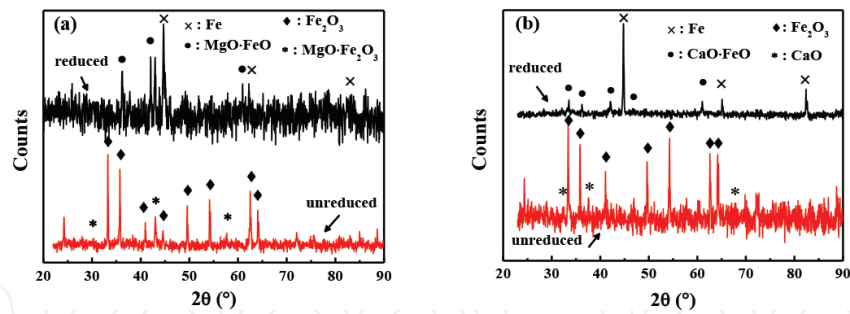


Figure 14. The XRD patterns of Fe_2O_3 particles before and after reduction (800°C , $74\text{--}149\ \mu\text{m}$, $24.3\ \text{cm/s}$): (a) adding 2% MgO and (b) adding 2% CaO.

be reduced to low-valent oxides, whereas the reaction rate was much lower than that of pure Fe_2O_3 . Therefore, the rate of surface metallization was decreased by adding MgO and CaO. Because the defluidization occurred at a critical metallization degree, agglomeration/defluidization was delayed by reducing the time to reach the critical metallization degree by adding MgO and CaO.

The composition and reducibility of the coating layers formed by adding MgO and CaO were different. For adding MgO, $\text{MgO}\cdot\text{Fe}_2\text{O}_3$ was observed, which was reduced to $\text{MgO}\cdot\text{FeO}$ based on XRD analysis. But the reduction of $\text{MgO}\cdot\text{FeO}$ to Fe hardly happens below 1100°C [36]. And the surface not only contains Fe and Mg, but also considerable O (**Figure 13(a)**), indicating the outer layer was mainly composed of oxides. Therefore, an unreduced coating layer in the formation of $\text{MgO}\cdot\text{FeO}$ generated on the surface, and thus prevented the contact of iron precipitated. As a result, the defluidization was inhibited. However, for adding CaO, the Fe oxides in the calciowustite coating can be reduced thermodynamically to metallic iron [37]; and the outer layer (**Figure 13(c)**) contains Fe, Ca, and a little O, suggesting that the phases of Fe were mainly metallic iron and a little oxide. It indicated that the calciowustite was reduced finally to iron. Therefore, the inhibition effect of Ca species can only temporarily inhibit defluidization. When metallic iron appeared on the surface, the defluidization occurred again. Thus, the inhibition effect of CaO on defluidization was less than that of MgO, especially at high temperatures

5. Conclusions

1. Particle cohesiveness and agglomeration tendency were initiated by metallization and depended strongly on the amount of iron precipitation. As the metallization degree increased, the fluidization behavior of Fe_2O_3 particles evolved from cohesiveness to sticky, and thus agglomeration appeared. The precipitation of metallic iron with submicro size was clearly identified as the necks on the Fe_2O_3 surfaces, which caused the formation of agglomerates.
2. Based on force balance, a quantitative model for the fluidization characteristics of iron powders was developed to describe the defluidization behavior at elevated temperatures. The theoretical model successfully predicted the defluidization temperature as a function of fluidizing gas velocity and gas properties. The simulated defluidization temperatures

were in a good agreement with the experimental results. According to the operating phase diagram of fluidization obtained by this model, the stable fluidization and the defluidization region were determined.

3. Mg- and Ca-coating Fe_2O_3 particles were shown to significantly extend the defluidization time, and this inhibition effect was increased by increasing the addition amount. A coating layer on the surface was found to mainly contain magnesiowustite ($\text{MgO}\cdot\text{FeO}$) and calciowustite ($\text{CaO}\cdot\text{FeO}$) generated by the reactions between Mg/Ca oxides and $\text{Fe}_2\text{O}_3/\text{FeO}$ during reduction process, and this coating layer was effective in preventing the connection of precipitated iron. And compared with CaO, MgO was more effective in delaying defluidization at the same conditions, because the unstable calciowustite was reduced to metallic iron and cannot completely suppress the precipitation of iron.

Nomenclature

A	Proportional constant for adhesion force	$\text{kg}^2\cdot\text{m}/\text{s}^4$
b	Radius of the connection between the particles	m
C_d	Drag coefficient	–
$(C_d)_{\text{mfs}}$	Drag coefficient in initial fluidization	–
d_p	Mean particle size	m
E_s	Activation of surface viscosity	J/mol
F_{ad}	Adhesion force	$\text{kg}\cdot\text{m}/\text{s}^2$
F_d	Drag force	$\text{kg}\cdot\text{m}/\text{s}^2$
K	Regressive constant	$\text{s}^4/(\text{kg}^2\cdot\text{m}^4)$
N_a	Number group for adhesion force	$\text{s}^2/(\text{kg}\cdot\text{m})$
$(N_a)_{\text{mfs}}$	Number group for adhesion force in initial fluidization	$\text{s}^2/(\text{kg}\cdot\text{m})$
N_d	Number group for drag force	$\text{kg}\cdot\text{m}^3/\text{s}^2$
$(N_d)_{\text{mfs}}$	Number group for drag force in initial fluidization	$\text{kg}\cdot\text{m}^3/\text{s}^2$
R	Gas constant	J/(K·mol)
Re	Reynolds number	–
T	Bed temperature	°C
T_{def}	Defluidization temperature	°C
$(T_{\text{def}})_{\text{cal}}$	Theoretical results of T_{def}	°C
$(T_{\text{def}})_{\text{exp}}$	Experimental results of T_{def}	°C
t	Connect time of two particles	S

U_g	Operating gas velocity	m/s
U_{mf}	Initial fluidizing velocity in nonsintering condition	m/s
U_{mfs}	Initial fluidizing velocity in sintering condition	m/s
α	Proportional constant for drag force	–
β	Proportional constant for connect time	m
μ_{s0}	Proportional constant for surface viscosity	Pa·s
μ_s	Surface viscosity	Pa·s
μ_g	Gas viscosity	Pa·s
ρ_g	Gas density	kg/m ³
ρ_s	Particle density	kg/m ³
σ	Tensile stress of agglomerate	Pa
δ	Relative error of T_{def}	%

Author details

Yiwei Zhong^{1*}, Jintao Gao¹, Zhancheng Guo¹ and Zhi Wang²

*Address all correspondence to: ywzhong@ustb.edu.cn

1 State Key Laboratory of Advanced Metallurgy, University of Science and Technology, Beijing, PR China

2 Institute of Process Engineering, Chinese Academy of Sciences, Zhongguancun, Haidian District, Beijing, PR China

References

- [1] Johannes LS. Recent status of fluidized bed technologies for producing iron input materials for steelmaking. *Particuology*. 2011;**9**:14–23
- [2] Komatina M, Gudenau HW. The sticking problem during direct reduction of fine iron ore in the fluidized bed. *Journal of Metallurgy*. 2004;**11**:309–328
- [3] Skrifvars BJ, Hupa M, Hiltunen M. Sintering of ash during fluidized bed combustion. *Industrial & Engineering Chemistry Research*. 1992;**31**:1026–1030
- [4] Seville JPK. High-temperature defluidization. *Powder Technology*. 1984;**38**:13–22
- [5] Compo P, Pfeffer R, Tardos GI. Minimum sintering temperatures and defluidization characteristics of fluidizable particles. *Powder Technology*. 1987;**51**:85–101

- [6] Seville JPK, Willett CD, Knight PC. Interparticle forces in fluidization: A review. *Powder Technology*. 2000;**113**:261–268
- [7] Bartels M, Lin W, Nijenhuis J, Kapteijn F, Ruud van Ommen J. Agglomeration in fluidized beds at high temperatures: Mechanisms, detection and prevention. *Progress in Energy and Combustion Science*. 2008;**34**:633–666
- [8] Hayashi S, Iguchi Y. Factors affecting the sticking of fine iron ores during fluidized bed reduction. *ISIJ International*. 1992;**32**:962–971
- [9] Gransden JF, Sheasby JS, Bergougnou MA. An investigation of defluidization of iron ore during reduction by hydrogen in a fluidized bed. *Chemical Engineering Progress*. 1970;**66**:208–214
- [10] Gransden JF, Sheasby JS. The sticking of iron ore during reduction by hydrogen in a fluidized bed. *Canadian Metallurgical Quarterly*. 1974;**13**:649–657
- [11] Zhong Y, Wang Z, Gong X, Guo Z. Sticking behavior caused by sintering in gas fluidisation reduction of hematite. *Ironmaking Steelmaking*. 2012;**39**:38–44
- [12] Mikami T, Kamiya H, Horio M. The mechanism of defluidization of iron particles in a fluidized bed. *Powder Technology*. 1996;**89**:231–238
- [13] Knight PC, Seville JPK, Kamiya H, Horio M. Modelling of sintering of iron particles in high-temperature gas fluidization. *Chemical Engineering Science*. 2000;**55**:4783–4787
- [14] Öhman M, Nordin A. A new method for quantification of fluidized bed agglomeration tendencies: A sensitivity analysis. *Energy Fuels*. 1998;**12**:90–94
- [15] Öhman M, Pommer L, Nordin A. Bed agglomeration characteristics and mechanisms during gasification and combustion of biomass fuels. *Energy Fuels*. 2005;**19**:1742–1748
- [16] Tardos GI, Mazzone D, Pfeffer R. Destabilization of fluidized beds due to agglomeration. Part 1: Theoretical model. *Canadian Journal of Chemical Engineering*. 1985;**63**:377–383
- [17] Buffington FS, Hirano K, Cohen M. Self-diffusion in iron. *Acta Metallurgica*. 1961;**9**:434–439
- [18] Himmel L, Mehl RF, Birchenal CE. Self-diffusion of iron in iron oxides and the Wagner theory of oxidation. *Transactions of the Metallurgical Society of AIME*. 1953;**197**:827–833
- [19] Tardos GI, Pfeffer R. Chemical reaction induced agglomeration and defluidization of fluidized beds. *Powder Technology*. 1995;**85**:29–35
- [20] Tardos GI. Measurement of surface viscosities using a dilatometer. *Canadian Journal of Chemical Engineering*. 1984;**62**:884–887
- [21] Zhong Y, Wang Z, Guo Z, Tang Q. Defluidization behavior of iron powders at elevated temperature: Influence of fluidizing gas and particle adhesion. *Powder Technology*. 2012;**230**:225–231
- [22] Satterfield CN. *Heterogeneous Catalysis in Industrial Practice*. 2nd ed. New York: McGraw-Hill; 1992

- [23] Hembree P, Wagner JB. Diffusion of Fe⁵⁵ in wustite as a function of composition at 1100°C. *Transactions of the Metallurgical Society of the American Institute of Mining, Metallurgical and Petroleum Engineers*. 1969;**245**:1547–1552
- [24] Benson SA, Jones ML, Harb JN. Ash formation and deposition. In: Smoot LO, editor. *Fundamentals of Coal Combustion-for Clean and Efficient Use*. Amsterdam: Elsevier; 1993
- [25] Seville JPK, Silomon-Pflug H, Knight PC. Modelling of sintering in high temperature gas fluidisation. *Powder Technology*. 1998;**97**:160–169
- [26] Turton R, Levenspiel O. A short note on the drag correlation for spheres. *Powder Technology*. 1986;**47**:83–86
- [27] Moseley JL, O'Brien TJ. A model for agglomeration in a fluidized bed. *Chemical Engineering Science*. 1993;**48**:3043–3050
- [28] Lin CL, Wey MY, Lu CY. Prediction of defluidization time of alkali composition at various operating conditions during incineration. *Powder Technology*. 2006;**161**:150–157
- [29] Kuo JH, Shih KM, Lin CL, Wey MY. Simulation of agglomeration defluidization inhibition process in aluminum-sodium system by experimental and thermodynamic approaches. *Powder Technology*. 2012;**224**:395–403
- [30] Hayashi S, Sawai S, Iguchi Y. Influence of coating oxide and sulfur pressure on sticking during fluidized bed reduction of iron ores. *ISIJ International*. 1993;**33**:1078–1087
- [31] Lin CL, Wey MY. The effect of mineral compositions of waste and operating conditions on particle agglomeration/defluidization during incineration. *Fuel*. 2004;**83**:2335–2343
- [32] Lin CL, Kuo JH, Wey MY, Chang SH, Wang KS. Inhibition and promotion: the effect of alkali earth metals and operating temperature on particle agglomeration/defluidization during incineration in fluidized bed. *Powder Technology*. 2009;**189**:57–63
- [33] Geva S, Farren M, St. John DH, Hayes PC. The effects of impurity elements on the reduction of wustite and magnetite to iron in CO/CO₂ and H₂/H₂O gas mixtures. *Metallurgical Transactions B (Process Metallurgy)*. 1990;**21**:743–751
- [34] Sesen MK. The influence of CaO on the precipitation behaviour of iron in the reduction of iron oxide. *Scandinavian Journal of Metallurgy*. 2001;**30**:1–7
- [35] Wang Z. *Ferrous Metallurgy*. 2nd ed. Beijing: Metallurgical Industry Press; 2002
- [36] Strellov KK, Safin IM, Fedotov VI. Reduction of iron oxide from commercial magnesite refractory. *Inorganic Materials*. 1981;**17**:1344–1347
- [37] Du S, Srinivasan NS, Staffansson LI. Reduction of calcium ferrites by hydrogen in the temperature interval 1191-1426 K. *Scandinavian Journal of Metallurgy*. 1988;**17**:233–238

